UNIVERSITY OF CALIFORNIA
RIVERSIDE

Effect of Strut Parameters on the Intra-Aneurysmal Hemodynamics of a Saccular Aneurysm on a Tortuous Parent Artery

A Thesis submitted in partial satisfaction
of the requirements for the degree of

Master of Science

in

Mechanical Engineering

by

Sanika Ravindra Nishandar

March 2019

Thesis Committee:

Dr. Masaru Rao, Chairperson
Dr. Marko Princevac
Dr. Monica Martinez-Wilhelmus

The Thesis of Sanika Ravindra Nishandar is approved:

_____

_____

_____

Committee Chairperson

University of California, Riverside

ACKNOWLEDGMENTS

I'd like to express my sincere gratitude to my advisor, Dr. Masaru Rao, for his continuous support, patience, and motivation throughout my master's study and research. The door to his office was always open whenever I had troubles or any questions regarding my research. I couldn't have imagined having a better advisor and mentor for my master's study.

The work presented in this thesis would not have been possible without the constant guidance of my seniors, Ryan Peck, and Benjamin Sommerkorn. I am grateful for all the support and knowledge they passed onto me throughout the period of my study. I thank my fellow lab mates in Biomedical Microdevices laboratory: Edver Bahena, Bryan Woo, Duncan Ashby, Samantha Corber, Pranee Pairs, Morgan Dundon and Kairui Xia for teaching me the lab culture and helping me out with my dissertation, presentations and my entire research in general.

I would also like to thank my seniors and friends, Rajasekhar Anguluri, Anand Katailiha, and Padmaja Jonnalagedda for their constant moral support and motivation even before I started working on my thesis. Last, but not least, I'd like to acknowledge the people who mean the world to me, my parents. Thank you for showing undying faith in me and giving me the freedom to choose what I desired. Finally, I'd like to extend my respect to both my grandmothers who believed in my ability to be successful in the academic arena. I consider myself fortunate to have such a great family, standing behind me with their love and support.

ABSTRACT OF THE THESIS

Effect of Strut Size and Stent Porosity on the Intra-Aneurysmal Hemodynamics in a Tortuous Parent Vessel Geometry: A Numerical Analysis

by

Sanika Ravindra Nishandar

Master of Science, Mechanical Engineering
University of California, Riverside, March 2019
Dr. Masaru Rao, Chairperson

Flow diverters are being increasingly used as an option of treatment for intracranial aneurysms. These devices are deployed endovascularly along the parent artery where an aneurysm is located. It takes advantage of the intra-aneurysmal hemodynamics to occlude the aneurysm by reconstructing the parent artery over time, replacing diseased tissue new healthy tissue. Although these minimally invasive, low porosity devices are being widely used for aneurysmal treatment, there are concerns around inefficiency associated with the high level of curvature in cerebral arteries. Some studies suggest that the inertia driven flow in tortuous arteries compared to the shear driven flow in the straight artery is the cause of inconsistent device performance. Previous research in our lab has indicated the potential of a novel microfabricated, solid construct balloon-deployable flow diverter within the posterior cerebral circulation. Presented herein, we demonstrate the effectiveness of these novel devices in tortuous parent arteries using computational fluid dynamic studies. We computed and compared the intra-aneurysmal hemodynamics for the stented and unstented cases of the tortuous geometry using ANSYS Fluent 18.2. The numerical results indicate higher flow velocities and wall shear stress

inside the aneurysmal sac as the tortuosity of the parent artery increases, which imply the presence of inertial flow in the tortuous models. Reduction of intra-aneurysmal velocity and wall shear stress are considered as the key hemodynamic parameters which promote thrombosis of aneurysmal tissue. Results after implantation of stents displayed substantially reduced values of inflow velocity and wall shear stress inside the aneurysm sac for all the studied models. Significant reductions were seen when high aspect ratio struts were computed at lower porosities in the straight as well as tortuous models. Values of velocity and wall shear stress reduction as high as 95% were observed with high aspect ratio struts at lower porosities. This indicates the efficient working of the high aspect ratio struts in the inertial flow regions of the tortuous parent arteries. The favorable outcome of this simulation is encouraging to further explore this device in more variations of aneurysm and parent vessel geometries.

TABLE OF CONTENTS

TABLE OF FIGURES

1. INTRODUCTION

1.1 Stroke and Aneurysm epidemiology

Cerebral aneurysms are blood filled dilations that bulge or balloon out on weak segments of a neurovascular artery mostly due to atherosclerotic disease or constant pressure from blood flow. The reason for the formation of an aneurysm, although vastly studied, remains largely unclear. Furthermore, most of the intracranial aneurysms are small and asymptotic and hence remain undiagnosed until they rupture and cause bleeding in the brain (Schievink, 1997). The medical condition wherein an aneurysm increases in size and ruptures causing bleeding in the brain is called a hemorrhagic stroke. Hemorrhage stroke accounts for about 13% of the total deaths by a stroke. It is known to be one of the prevailing causes of death and disability (An, Kim, & Yoon, 2017). Depending on the location of the bleeding, an intracerebral hemorrhagic stroke can be classified as parenchymal stroke (bleeding inside the parenchymal tissue of brain) and Subarachnoid stroke (bleeding in the subarachnoid space) (Keedy, 2006).

The incidence of Intracranial aneurysms is relatively common, ranging from approximately 4% - 6% of the total population (Keedy, 2006). Data collected (Schievink, 1997) suggests that the occurrence of aneurysmal subarachnoid hemorrhage has not changed significantly from the 1950s to the 1980s and the fatalities due to rupture of aneurysms in the 1990s were approximately 14,000 people annually. According to Aneurysm Stroke Foundation as of 2015, stroke ranks 5th among all causes of death, killing almost 140,000 people annually, which accounted for approximately 1 out of every 19

deaths in the United States (Benjamin et al., 2018). This suggests that even after diagnostic and surgical advances, the incidence of deaths by rupture of the aneurysm has remained approximately the same.

1.2 Aneurysm anatomy and classification

Aneurysms are classified based on their shape, size, and location of incidence. Based on their shape, cerebral aneurysms are broadly categorized as Saccular and Fusiform aneurysms. These categories are shown in Fig 1 (Withers, Carolan-Rees, & Dale, 2013). Saccular or berry aneurysms, as the name suggests, are pouch-like dilations on a small portion of the arterial wall and account for a total of 90% of all the types of aneurysms (Frösen et al., 2012; Keedy, 2006). The blood-filled sac of the berry aneurysm is connected to the artery by a narrow opening called the neck. Alternatively, Fusiform aneurysms are dilations involving the entire circumference along the length of the vascular wall (Massoud et al., 1995).

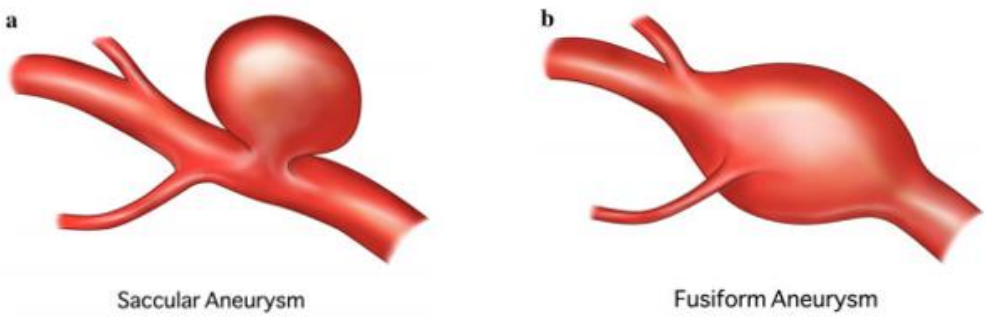

Figure 1: Representation of saccular (a) and fusiform (b) aneurysms (Withers et al., 2013)

Additionally, saccular aneurysms are classified based on the diameter of the diseased tissue called the sac. Generally, aneurysms with a sac diameter of less than $10\ mm$ are classified as small aneurysms. These small aneurysms are usually benign and can go undiagnosed throughout the person's life. On the other hand, aneurysms with a sac diameter greater than $10\ mm$ are classified as large or giant aneurysms and are at a higher risk of rupture and have to be treated (Greving et al., 2014). Studies have tried to prognose the rupture of an aneurysm, not only based on the size of the aneurysm but also the location of its incidence (Korja, Kivisaari, Rezai Jahromi, & Lehto, 2016). According to the studies that relate the growth and rupture of aneurysms to the location of incidence, approximately 90% of cerebral aneurysms form in the anterior circulation while the remaining 10% form in the posterior circulation. More specifically, in the anterior circulation, around 20% of aneurysms develop in the middle cerebral arteries, 30% in the internal carotid arteries, and 30%–35% in the anterior communicating artery (Vega, Kwoon, & Lavine, 2002). Approximately, half of the aneurysms in the posterior circulation develop at the basilar apex, and the remaining half in the arteries, such as the superior and inferior cerebellar arteries, the posterior inferior cerebellar arteries, and vertebrobasilar junction (Savastano, Bhambri, Andrew Wilkinson, & Pandey, 2018). Fig 2 shows the locations at which the intracranial aneurysms develop frequently (Vega et al., 2002).

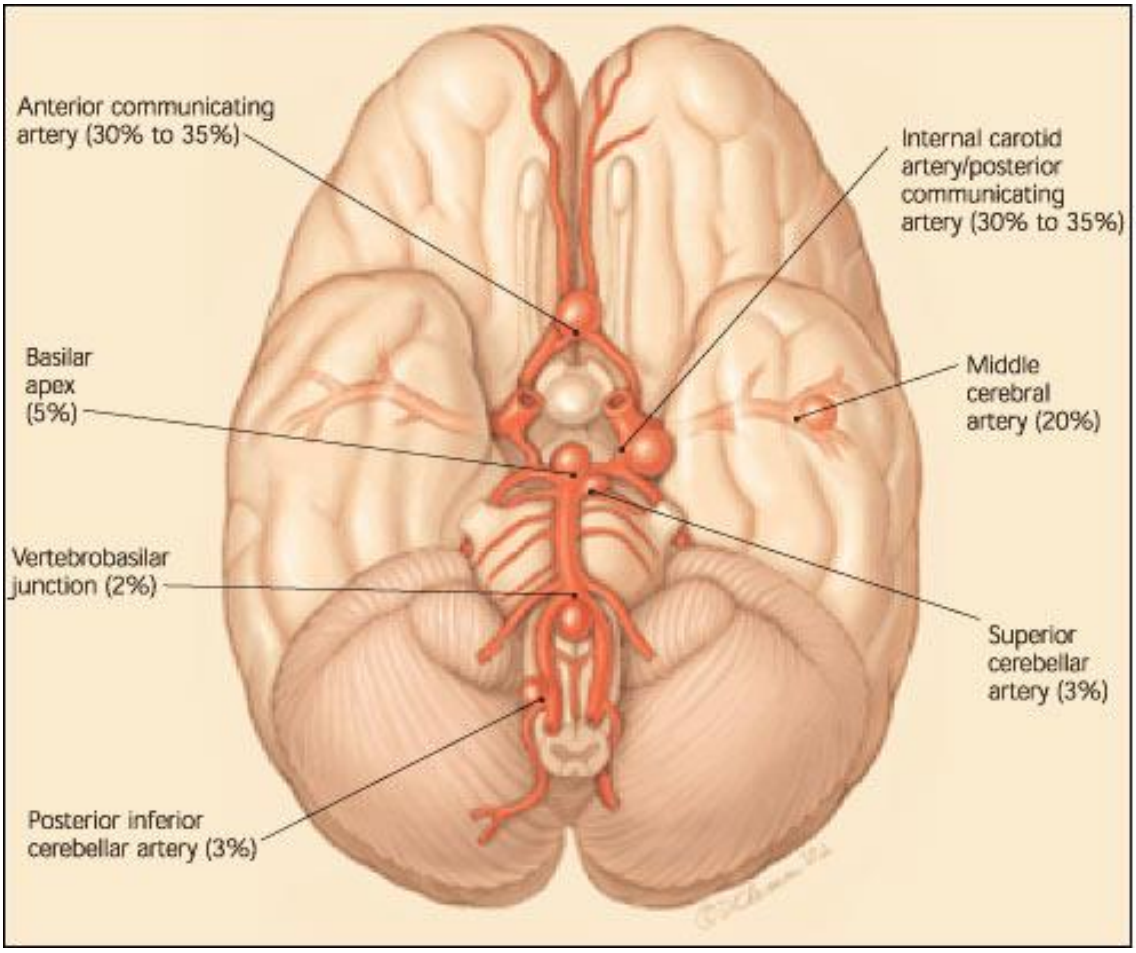

Figure 2: Frequent locations of intracranial aneurysms (Vega et al., 2002)

1.3 Symptoms, Causes, and Diagnosis of cerebral aneurysms

Aneurysms are mostly asymptotic and can go undiagnosed throughout the person's life until they become large or rupture. While growing, the aneurysms may exert pressure on the peripheral nerves and tissues and may cause extremely severe headache and other symptoms such as nausea, impaired vision, seizures, paralysis, light sensitivity, confusion, and loss of consciousness.

The mean age of patients with aneurysmal subarachnoid hemorrhage is around 50 years, but the incidence of hemorrhage increases with age until at least 80 years of age (Schievink, 1997). Moreover, the incidence of an aneurysm has been detected at a larger percentage in the female population. A family history of SAH, smoking, hypertension, and autosomal polycystic kidney disease are the most salient epidemiological causes for intracranial aneurysm development.

Cerebral aneurysms are usually diagnosed by imaging tests when the patient displays most of the symptoms in conjunction. The imaging tests include CTA (computed tomographic angiography) and MRA (magnetic resonance angiography), which are non-invasive, and cerebral angiogram, which is minimally invasive.

1.4 Treatment options for Stroke Prevention

1.4.1 History of Aneurysmal Surgery

The first reported case of surgical treatment for intracranial aneurysms was carried out by Dr. Walter Dandy in 1937. Dr. Dandy operated on a pea-sized aneurysm arising from the internal carotid artery, adjacent to the entry of posterior communicating artery in a patient with a third- nerve palsy. In this craniotomy approach, Dr. Dandy ceased the blood supply to the aneurysm by placing a silver clip at the neck and thrombosed the aneurysmal sac by electrocautery (Dandy, 1938). Craniotomy and clipping have been used as effective gold standard surgical treatments for cerebral aneurysms since their inception for almost 80 years. Various advancements have been made over the years such as the introduction of microsurgery with an operating microscope, intraoperative monitoring and modifications in clips by the inclusion of springs and serrated teeth (ISHIKAWA, 2010). Although clipping provides complete occlusion and prevents re-bleeding, it is limited to surgical accessibility of the aneurysm and is inefficient in large volume aneurysms. Thus, research has drifted towards endovascular devices such as balloon catheters, coils, and flow diverters.

1.4.2 History of Endovascular Treatment – Coil Embolization

To address the issues of invasiveness, accessibility, and significant recovery time, an era of endovascular treatments was brought about by the advent of the Seldinger technique, commonly referred to as catheterization (Seldinger, 1953). With the success of this non-intrusive technique, the use of implantable latex balloons deployed by a catheter for management of cerebral aneurysm was first reported by Serbinenko in the 1970s (Serbinenko, 1974). Further advancement included the design of detachable silicone and latex balloons, but this procedure displayed high rates of surgical morbidity (David Fiorella, MD, Ph.D.; Michael E. Kelly, MD; Raymond D. Turner IV, MD; and Pedro Lylyk, 2008). Alternatively, atraumatic and safely deployable embolization coils were introduced in the 1990s. The widely used Guglielmi Detachable Coil (GDC) system got FDA approval in 1995. These GDC's are soft detachable platinum coils, which are navigated and positioned in the aneurysmal sac with the help of a microcatheter. A soldered stainless-steel guidewire is supplied with a low direct electric current which helps to initiate thrombosis in the aneurysm. The thrombosis was the result of the attraction of the negatively charged red and white blood cells, platelets, and fibrinogen to the positively charged platinum coils (Guglielmi, Viñuela, Sepetka, & Macellari, 1991). With further advancements, coils that formed dense basket-like webbing inside the aneurysmal sac were introduced. Although these coils efficiently aided thrombosis, there can be complications such as unintentional parent vessel occlusion. Furthermore, a lack of any

neck structures in wide-necked and fusiform aneurysms make coil placement very tenuous.

1.4.3 Flow Diverter Treatment

The concept of using flow diverters (FD) as a treatment for cerebral aneurysms is fairly new and was proposed by Higashida et al in the 1990s, wherein a fusiform aneurysm on basilar artery was treated using a coronary stent. FD's are tubular implants of densely braided wires, which reduce the risk of the aneurysm using a multi-faceted mechanism. Theoretically, FD's are devices that promote endoluminal reconstruction instead of endosaccular filling. The mechanism in which the flow diverters work consists mainly of three stages: flow stagnation, transient thrombosis, and neointimal remodeling.

Flow Disruption: The placement of the FD across the neck of the aneurysm reroutes the blood flow and reduces the radial in-flow towards the aneurysmal sac. This is an immediate effect after the placement of the FD. This disruption in flow decreases the velocity, vorticity and wall shear stress (WSS) inside the sac, which in turn lowers the risk of rupture. Although the flow is curtailed, the aneurysm tissue and the adjoining perforating arteries can continue to access the nutrient from the parent artery due to the porous nature of the stents.

Thrombosis of diseased tissue: After the flow is disrupted, FDs lead to changes in aneurysmal hemodynamics that promote thrombosis, which eventually occludes the aneurysm from circulation. The occlusion takes the course for a period of a few months after which the endoluminal layer forms over the stents reconstructing the parent tissue.

Neointimal Modeling: The final stage occurs after complete occlusion of the aneurysmal tissue. In this stage, the endothelialization occurs on the device mesh, which acts as a scaffold. Furthermore, the occluded tissue is dissolved in the surrounding tissue and the aneurysm is eventually resorbed.

However, there are a few drawbacks with using FD as the treatment for cerebral aneurysms. Perforator occlusion, in-stent thrombosis, perianeurysmal edema, and delayed hemorrhages are some of the risks associated with FD's (Alderazi et al., 2014). Moreover, a monitored and tailored antiplatelet therapy is mandatory, potentially for an indefinite amount of time.

1.5 Hemodynamics of Cerebral Aneurysms

Among the physiological and morphological factors, hemodynamics are the main predictors of aneurysm formation and rupture. Hemodynamic studies investigate the blood flow dynamics, taking into consideration the physical laws that govern the blood flow in arteries. The two key hemodynamic factors are velocity and pressure. Increase in velocity increases the WSS on the arterial walls, which can cause damage to the vasculature. Increase in pressure, which is medically termed as hypertension, is one of the major diagnoses for aneurysm formation and consequently a stroke. Over the years, various studies have been conducted to better understand the hemodynamics involved in initiation, growth, rupture, and treatment effectiveness related to cerebral aneurysms (Alkhalili et al., 2018; Chung & Cebral, 2014). Most commonly investigated hemodynamic parameters are viscosity and composition of blood, flow velocity, volumetric flow rate and intra-aneurysmal pressure (Castro, Akan, Kim, & Souftas, 2013). Moreover, studies have also been conducted using Non-Newtonian blood flow, gravitational forces, steady and pulsatile flows, and elasticity of parent vessel walls (Coussement et al., 2016; Mach, Sherif, Windberger, Plasenzotti, & Gruber, 2016; Torii, Oshima, Kobayashi, Takagi, & Tezduyar, 2007).

The effectiveness of flow diverters and their impact on aneurysms has been heavily researched. People have investigated the influence of flow diverters in terms of porosity, strut width, strut shape, parent morphology, and various other aspects. Flow patterns,

velocity, pressure and their derived quantities such as WSS reduction, Relative residual time (RRT), vorticity and oscillatory shear index (OSI) are a few of the parameters commonly evaluated to ascertain the efficient working of the FD's. OSI is a dimensionless metric that characterizes the alignment of the wall shear stress vector with the transverse wall shear stress vector throughout the cardiac cycle. Whereas, RRT demonstrates the residence time of the fluid particles adjacent to the wall, which when increased, increases the particle deposition and inflammatory response in that area (Riccardello et al., 2018). In general, FDs divert the flow away from the aneurysm and that in turn reduces the velocity of flow in the sac, which results in a reduction of wall shear stress (WSS) at the wall. Moreover, studies concluding reduction in RRT, OSI and vorticity due to FD's have also been reported (Lv et al., 2018; Zhao et al., 2017).

1.6 Tortuosity of Cerebral Vasculature

1.6.1 Importance of studying tortuosity

Morphology of aneurysms has been determined to be a significant determinant for varied hemodynamic patterns in the aneurysm geometry by several studies (Skodvin, Johnsen, Gjertsen, Isaksen, & Sorteberg, 2017). Investigations have been conducted on the influence of aneurysm shape, size, and the angle of flow. However, the morphology of the parent vessel and specifically tortuosity of the parent vessel is one of the morphological parameters which hasn't been explored much. The curvature of vessels in cerebral vasculature often results in malposition of the FDs and can cause inefficient performance even when correctly positioned. The porosity of the device also varies from the one envisioned during implantation. In a computational study using a varying radius of curvature, (Meng et al. (2006) observed that as the curvature of the parent vessel increases, the flow changes from a shear driven one to an inertial flow of higher velocity, which is directed towards the aneurysmal cavity. Furthermore, the region of WSS on the distal wall of the sac increases, which might trigger an early rupture. The magnitudes of velocity and vorticity were also determined to be three to four times higher in the inertial flow model than the shear driven flow model in PIV studies (Augsburger et al., 2009). It was also discerned that the velocity reduction and vorticity reduction in tortuous arteries after placement of FD's are not as efficient as in the straight ones (Kim, Taulbee, Tremmel, & Meng, 2008).

1.6.2 Internal Carotid Artery as a study model

In a study by Pia (1980) regarding large aneurysms, in all of the cerebral circulation, about 50 percent of giant aneurysms were situated on the internal carotid artery. Giant aneurysms (Sac diameter > 2.5mm) are often symptomatic and can easily be diagnosed by angiography. The large diameter and dome-to-neck ratio of these aneurysms make them the best candidates for flow diversion treatment. Moreover, Passerini et al. (2012) observed the association of ICA arterial bends of ICA with the increased risk of rupture. Furthermore, Kliś, Krzyżewski, Kwinta, Stachura, & Gąsowski (2019) and Lauric, Hippelheuser, Safain, & Malek (2014) correlated ICA geometry with the development and presence of aneurysms. The ICA geometry consists of various segments as classified by Bouthillier, but the cavernous segment is the one with a maximum number of bends. Fig 3 shows a schematic of the internal carotid artery (Gilroy, MacPherson, & Ross, 2008). The cavernous segment of ICA extends from the petrolingual ligament to the dural ring in a characteristic S shape defined by two distinct bends: anterior genu, and posterior genu, connected by a horizontal segment. This S shape is commonly referred to as the carotid siphon and has angles ranging upwards of 90˚. Furthermore, the S-shaped Carotid in itself is classified to have varied shapes such as the U shape, V shape, C shape, and an arc shape as shown in Fig 4 (Lin et al., 2015; Pu et al., 2012). The highly tortuous nature of ICA and the precedence of being susceptible to aneurysm formation make it an appropriate candidate for studying the effect of tortuosity.

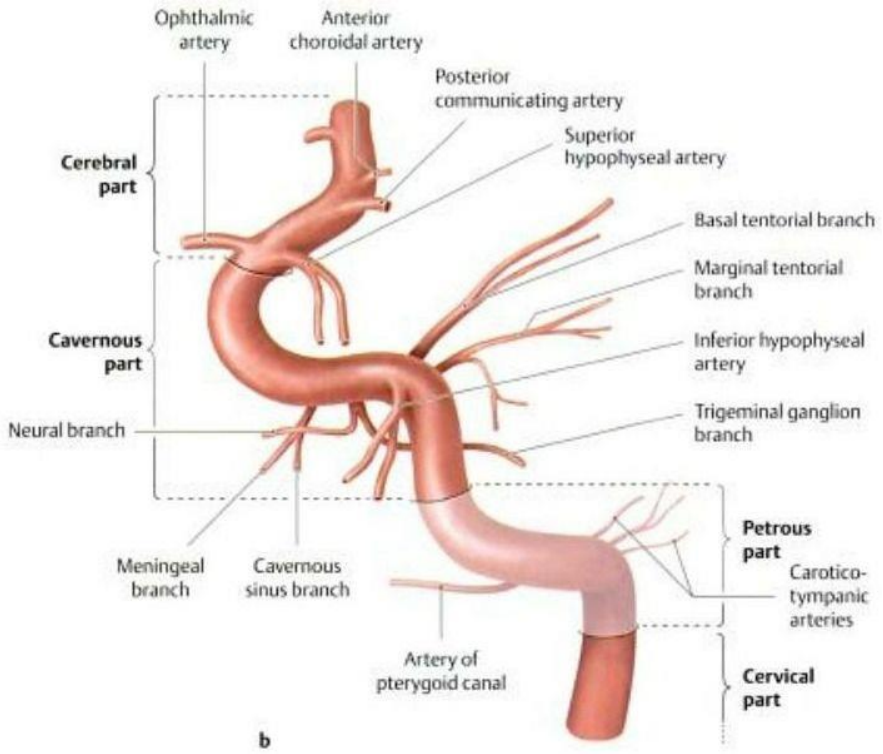

Figure 3: Schematic of an Internal Carotid Artery. (Gilroy, Anne M, Brian R. MacPherson, and Lawrence M. Ross. Atlas of Anatomy. Stuttgart: Thieme, 2008)

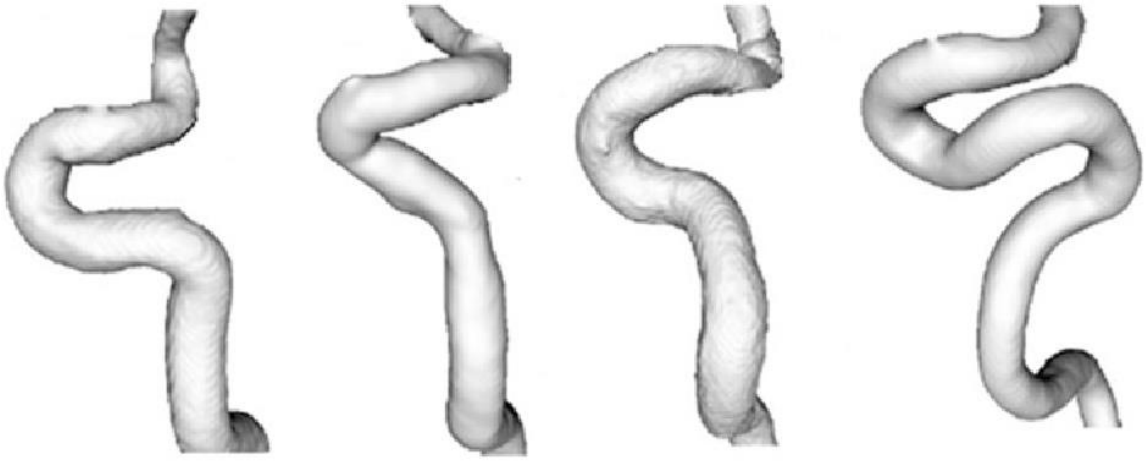

Figure 4: Different shapes of carotid siphon (Pu et al., 2012)

1.7 Thesis Motivation, objective and structure of the report

The motivation behind this work was the creation of novel, solid, microfabricated, rectangular, high aspect-ratio (AR) Flow diverter designed by Ryan Peck (Biomedical Microdevices Laboratory, University of California, Riverside). Furthermore, a report by Benjamin Sommerkorn (Biomedical Microdevices Laboratory, University of California, Riverside) demonstrated comparably better flow reduction by these struts compared to the state-of-the-art pipeline embolization devices.

This report is an attempt at further strengthening the conclusion conferred from the aforementioned studies by implementing the high aspect ratio FD devices in different parent morphology. The said tortuous morphology has proven to diminish the performance of FD devices considerably. The objective of this report is twofold:

1. Quantifying the changes in aneurysmal hemodynamics due to tortuosity in the parent artery.
2. Validating the amount of flow reduction of high aspect-ratio struts in tortuous parent morphologies.

The thesis primarily contains five chapters as explained. Chapter 1 “Introduction” contains background information regarding the epidemiology, classification, and treatments for cerebral aneurysms. Chapter 2 “Background on Computational Fluid Dynamics” gives comprehensive information on the CFD approach used in this study. Chapter 3 “Methodology” describes the geometry and physical parameters used for the problem. Chapter 4 “Results and Discussion” illustrates the objectives of the thesis and finally Chapter 5 “Conclusion and Future Direction” discusses the limitations of this study and presents ideas for further research.

2. BACKGROUND ON COMPUTATIONAL FLUID DYNAMICS

2.1. Introduction

Computational Fluid Dynamics (CFD) is a numerical approach for simulating fluid flows, which provides a non-invasive way of predicting the effect of flow diverters on the local hemodynamics in the aneurysmal sac and the parent vessel. A CFD analysis is carried out in the following three steps:

1. Pre-processing – Firstly, the geometry of the model is established using an inbuilt application (Design Modeler, in this study) and boundaries such as walls, interiors, inlets, and outlets are defined. The domain is then discretized into a finite number of control volumes or elements, using a computational grid called the mesh. The mesh is then imported to ANSYS FLUENT, where the properties of the fluid (viscosity, density) and the boundary conditions such as inlet velocity and mass flow rate are defined.
2. Processing – Based on the input parameters FLUENT implements the governing equations on individual control volumes and algebraic equations for dependent variables such as velocities and pressure are formulated. The discretized governing equations are linearized, and solution of the resultant linear equation system yields updated values of velocity and pressure fields.

3. Post-processing – Once the processor generates the flow fields, they are exported to data processors (CFD-Post, Excel) to generate plots and contours for better understanding the flow in the domain. These stages are explained in detail in this chapter.

2.2. Meshing, Residual Convergence, and Mesh Independence

In ANSYS Mesher, a continuous domain in any problem is discretized into finite control volumes called elements. These elements together form a grid-like structure commonly termed as a mesh. The fluid flow variables are applied to all the grid points in a discretized domain as in Fig 5 (ANSYS Fluent Tutorial Guide, 2015).

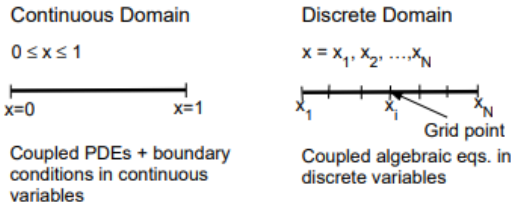

Figure 5: Discretization of flow domain in finite elements. (ANSYS Fluent Tutorial Guide, 2015)

A mesh can be uniform (all elements have the same geometry and dimensions) or a non-uniform depending on the geometry that is used. A 2D mesh can have triangular, quadratic elements or a combination of both. Similarly, a 3D mesh can have a hexahedral, tetrahedral, pyramid, wedge, and polyhedral elements. Furthermore, the mesh elements can be linear, quadratic (mostly preferred) or hybrid configuration as in Fig 6. Quadratic

elements provide a greater number of nodes with the same number of elements as in the linear configuration, and in turn, produce a better quality of results at small mesh volumes. The governing equations of mass and momentum are applied at the nodes of these elements.

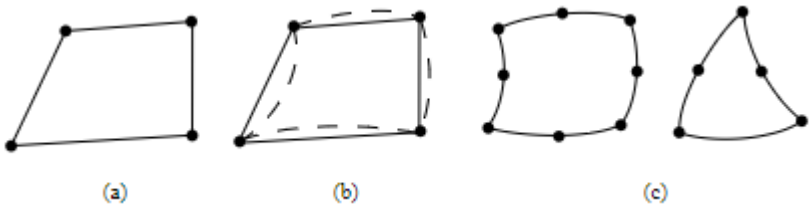

Figure 6: (a) Linear isoparametric, (b) Linear isoparametric with extra shapes and (c) Quadratic (ANSYS Fluent Tutorial Guide, 2015)

For all the meshes, combinations of different parameters such as cell size, mesh volume, mesh resolution, and orthogonal quality are evaluated. Mesh size or volume can be controlled using features such as element size and element inflation.

After meshing, the continuity of the flow across subdomains must be ensured for accurate results. One of the ways to ascertain the continuity of the flow is monitoring the residual convergence. Residuals signify the local imbalances of the conserved field variables such as mass and momentum in the discretized control volumes. The convergence history is saved by the solver by computing and storing the residual sum of the conserved variables at the end of each iteration (*ANSYS Fluent Tutorial Guide*, 2015). Therefore, the solution is more accurate when the residuals are low, and the solution is converged.

Finally, a mesh is said to be accurate when the solver provides results using a minimum number of elements and the results are independent of the volume (mesh size). Hence, mesh independence studies are conducted to ensure that the results of the simulation are independent of mesh size. In the mesh independence study, one of the outputs is compared across varying mesh size. The mesh size is usually double that of the previous equation and the outputs are compared until the variation in the value of the output is under the desired error margin.

2.3. Background on Ansys FLUENT

Ansys FLUENT is a finite volume-based solver that uses a pressure-based approach for low speed and incompressible flows. In this approach, the pressure and velocity fields are obtained by solving the conservation of mass and momentum equations. The equations for continuity and conservation of momentum in an inertial (non-accelerating) reference frame are as follows:

Conservation of mass - Continuity equation:

$$\frac{\partial \rho}{\partial t} + \nabla . (\rho \vec{v}) = 0 \quad (1)$$

Where v is the fluid velocity and ρ is the density.

Conservation of momentum equation:

$$\frac{\partial}{\partial t}(\rho \vec{v}) + \vec{v} \cdot \nabla \vec{v} = -\nabla p + \nabla \cdot (\bar{\bar{\tau}}) + \rho \vec{g} + \vec{F} \quad (2)$$

Where v is the fluid velocity, ρ is the density, p is the static pressure, $\bar{\bar{\tau}}$ is the tress tensor, $\rho\vec{g}$ is the gravitational force and $\vec{F}$ takes into account the external body forces.

The Integral form of conservation of mass used over the control volume of each cell is:

$$\frac{d}{dt}\iiint_V \rho\, dV = -\oiint_A \rho\vec{v}\cdot\hat{n}\, dA \tag{3}$$

Where the term on the left denotes the rate of change of mass and the term on the right is the net inflow of mass.

Applying Gauss's theorem,

$$\iiint_V \left[\frac{\partial\rho}{\partial t} + \nabla\cdot(\rho\vec{v})\right] dV = 0 \tag{4}$$

Similarly, the Integral form of conservation of momentum used over the control volume of each cell is:

$$\frac{d}{dt}\iiint_V \rho\vec{v}\, dV + \oiint_A \rho(\vec{v}\cdot\hat{n})\vec{v}\, dA = -\oiint_A P\hat{n}\, dA + \iiint_V \rho\vec{g}\, dV + \vec{F} \tag{5}$$

Rate of change of momentum | Net inflow of momentum | Total pressure | Total body forces

Applying Gauss's theorem, the x component of integral conservation of momentum can be written as,

$$\iiint_V \left[\frac{\partial\rho u}{\partial t} + \nabla\cdot(\rho u\vec{v}) + \frac{\partial P}{\partial x} - \rho g_x - F_x\right] dV = 0 \tag{6}$$

Lastly, the stress tensor is calculated as follows:

$$\bar{\bar{\tau}} = \mu\left[(\nabla\vec{v} + \nabla\vec{v}^{T}) - \frac{2}{3}\nabla\cdot\vec{v}I\right] \quad (7)$$

Where μ is the molecular viscosity, I is the unit tensor, and the second term on the right-hand side is the effect of volume dilation.

Although velocity field is derived directly from the momentum equation, the pressure fields are obtained by solving pressure or pressure correction equations.

These pressure equations are integral forms of the steady-state continuity and momentum equations as shown below:

$$\oint \rho\,\vec{v}\cdot d\vec{A} = 0 \quad (8)$$

$$\oint \rho\,\vec{v}\vec{v}\cdot d\vec{A} = -\oint pI\cdot d\vec{A} + \oint \bar{\bar{\tau}}\cdot d\vec{A} + \int_{V}\vec{F}\,dV \quad (9)$$

Where v is the fluid velocity, ρ is the density, p is the static pressure, $\bar{\bar{\tau}}$ is the tress tensor, I is the unit tensor and $\vec{F}$ takes into account the external body forces.

2.4. Post Processing

The final step of any CFD analysis is the visualization of the output variables. The results obtained from the results are plotted in terms of contour plots, vector plots or streamlines for a better understanding of the flow fields.

3. METHODOLOGY

3.1 Parent Vessel and Aneurysm Geometry

The recent trend in CFD studies is to use patient-specific models. Although, patient-specific models seem to give a better insight on the hemodynamics in the real human body, determining the effect of specific geometric characteristics on the blood flow is difficult. Thus, a parametric study with an idealized geometry can better demonstrate the relationship between the geometric characteristics and the hemodynamics in the model. Fig 7 shows an idealized 2D model of a sidewall aneurysm on an internal carotid artery that was used in the CFD simulations. The model comprises of a circular aneurysmal sac of radius R = 3mm, neck width W = 4.5mm and neck height H = 1.5 mm. The diameter of the aneurysm used for the study was chosen based on literature that has shown an increased incidence of rupture (Jeong, Jung, Kim, Eun, & Jang, 2009). The dome-to-neck ratio of DNR = 1.33 was considered.

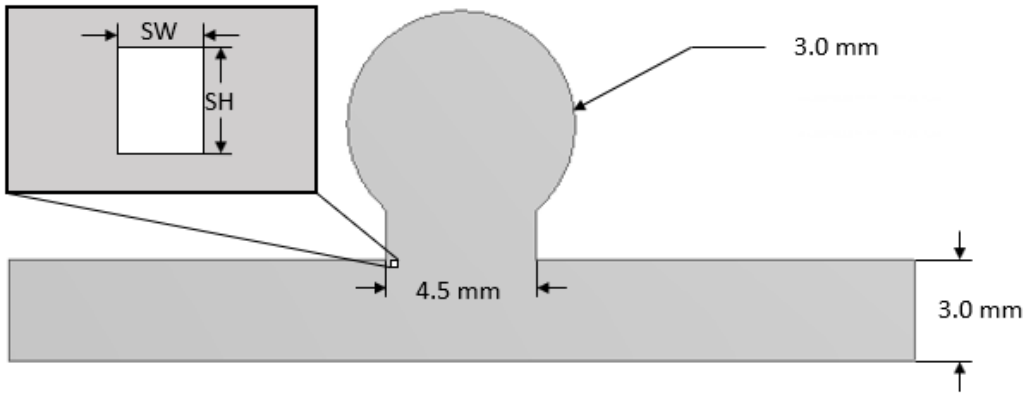

Figure 7: Aneurysm, Parent Vessel and Stent Geometry. SW is held constant at .30mm while SH is varied.

Flow diverters have been commonly recommended for DNR's less than 1.5 (Nelson et al., 2011). The diameter of the parent vessel (D) is taken as 3 mm.

Additionally, the parent length is extended to 10 times the vessel diameter on both sides, to ensure developed flow before entering the aneurysm. This geometry for the parent artery is consistent with Internal Carotid Artery, which has been known to have a high prevalence of aneurysms and more arterial bends than other arteries in the cerebral vasculature (Lin et al., 2015). For the tortuosity study the angle of curvature is altered from 0 – 180 degrees, as demonstrated in Fig 8. This range takes into consideration the curvature of most of the arterial bends in ICA. Additionally, keeping the arc length fixed enables quantification of the effect of the angle of curvature over a fixed segment size.

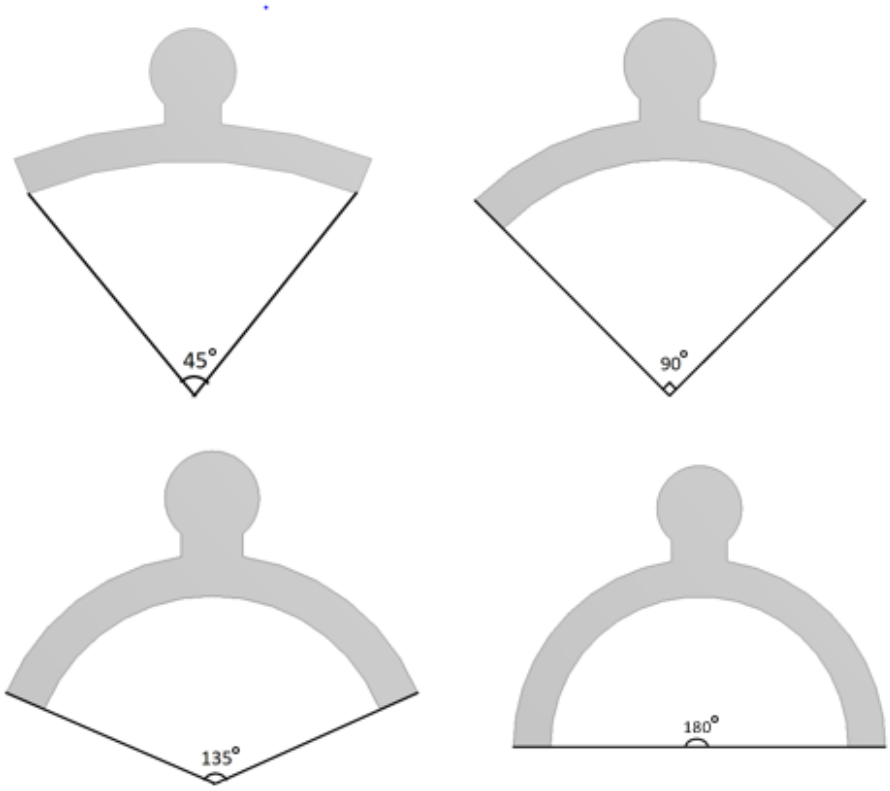

Figure 8: Ideal geometry of parent vessel with varying angle of tortuosity.

3.2 Stent Geometry

Rectangular struts are considered for this study as shown in Fig 6. It has been seen that modifying the width of the struts decreases the porosity but has a negligible effect on aneurysmal vorticity reduction (Xu & Lee, 2009). Consequentially, previous studies conducted in our lab showed that altering the height of the struts provides efficient velocity and vorticity reductions (Peck, 2015). Thus, in this study, the width of the strut (SW) is kept constant at 0.03mm and the strut height (SH) is varied from 0.015 mm to 0.09mm. Furthermore, the results for each strut height have been computed for 60%, 70%, 80%, and 90% porosities. The porosity was altered by changing the gap size between the struts as well as the number of struts covering the neck.

3.3 Meshing & Mesh Independence

Mesh volume of 20 thousand and 200 thousand elements was generated for the unstented and stented case respectively. The mesh volume was manipulated using mesh controls such as element size and inflation. Furthermore, the inflation controller was set to 5 layers along the wall, which increases the accuracy of boundary results such as WSS. Finally, the mesh was set to have hybrid elements (linear and quadratic) for more accurate results.

It is important in a computational fluid dynamic study to ascertain that the results are independent of the mesh size. Hence, a mesh independence study was conducted by increasing the mesh size while gradually decreasing the element size from 0.5 mm to

0.03mm. The mesh independence was compared against the intra-aneurysmal velocity. The simulation was considered mesh independent when the residuals were below 1×10^{-6}, which is three orders of magnitude lower than the magnitudes of velocity, measured in this simulation. An accuracy of 5% or less was reached.

3.4 Boundary Conditions for the CFD simulation

Blood is modeled as a Newtonian fluid with dynamic viscosity μ = 3.5 cP and density ρ = 1060 kg/m^3. Although blood is known to display Non-Newtonian properties, it is only in the region where hematocrit is high. This region is typically observed in microcirculation where the diameter of the vessel approaches the length scale of blood-borne cells. The diameter of the vessel considered in this study does not fall in this submillimeter scale. The blood flow is modeled as laminar and incompressible as the Reynolds number ($Re = \rho VL/\mu$), is small in the cerebral vasculature. All these parameters mentioned, are widely used in the computational modeling of similar studies. A volumetric flow rate of 257 ± 48 mL/min was considered based on the flow in ICA geometry (Zarrinkoob et al., 2015). Corresponding to this volumetric flow rate, an inlet steady-state flow velocity of 0.606 m/s was calculated. A steady-state model with mean volumetric flow rate at peak systole can be considered as the Womersley number, $\alpha = R\sqrt{\omega\rho/\mu}$, in the cerebral vasculature is close to unity. Wormersley number is a dimensionless number that relates the pulsatile flow frequency to viscous effects in the modelling of blood circulation.

No-slip boundary conditions are applied to the wall and the outlet is set to zero gauge pressure. Considering all the boundary conditions the equations mentioned in section (2.3) can be modified as follows:

Conservation of mass - Continuity equation:

$$\nabla . v = 0 \tag{1}$$

Conservation of momentum equation:

$$\rho\left(\frac{\partial v}{\partial t} + \ v \cdot \nabla v\right) = \ -\nabla p + \ \mu\nabla^2 v \tag{2}$$

4. RESULTS AND DISCUSSION

This chapter demonstrates the results of the simulations in accordance with the problem formulation in the previous chapter. The angle of curvature of the parent vessel is varied as mentioned in the methodology to assess the effect of tortuosity on the intra-aneurysmal hemodynamics, specifically average velocity, and average WSS. Furthermore, porosity and strut height of the stents are varied simultaneously to determine the influence of aspect-ratio (AR) and porosity on the aneurysmal hemodynamics.

4.1 Aneurysmal Hemodynamics due to tortuosity in Parent Artery: Pre-Stenting

Fig 9 shows the contour plots of velocity profile inside the aneurysmal sac of all the studied cases, wherein the direction of flow in the parent artery is from left to right. In all the cases, inlet flow impinges on the distal end of the sac. It can be seen that as the tortuosity increases from 0 to 180 degrees, the flow transits from shear driven flow to

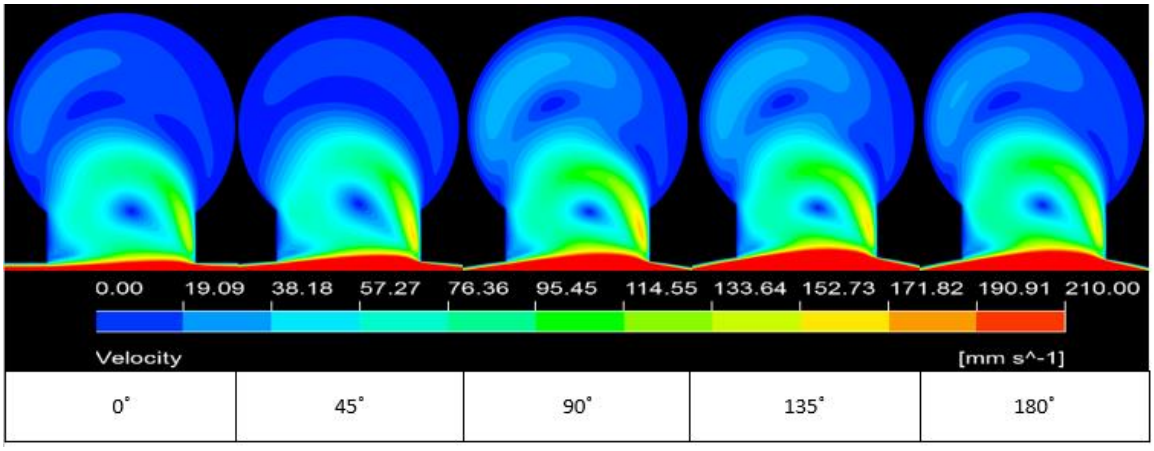

Figure 9: Contour Plot of velocity with increasing angle of tortuosity. As the angle of tortuosity increases, the flow becomes inertial then causing the larger part of the neck to be subjected to higher velocity. The formation of vortex as the angle increases signifies that the re-circulation increases with increase in angle of tortuosity.

inertia driven flow. These results are consistent with prior PIV studies by Augsburger et al. (2009). Consequently, it can be seen in Fig 10 that the maximum velocity inside the sac increases as the tortuosity of the parent vessel increases, which is in accordance with the results from previous studies on the tortuosity of the parent vessel (Meng et al., 2006). The change in velocity is not noticeable until the angle reaches 45˚. The maximum velocity increases, until the angle of curvature, reaches 90˚ and then reduces back again. However, the maximum velocity in the case of 180˚ is still greater than that of the straight case. This suggests that the aneurysm is most vulnerable to rupture when the tortuosity of the parent vessel is 90˚. But, the average velocities decrease as the angle increases. The increase in the magnitude of the maximum velocity implies the change of flow from shear driven to inertia driven. Fig 10 compares the magnitudes of the velocities.

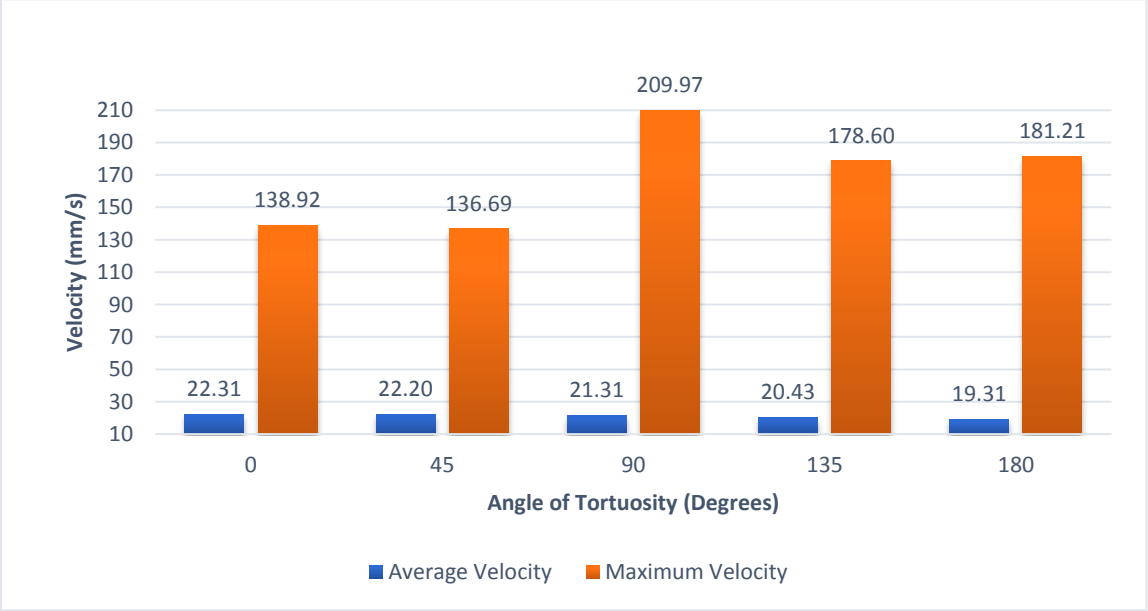

Figure 10: Bar Graph depicting the difference in the magnitudes of Maximum velocity and Average velocity with increase in angle of tortuosity of the parent vessel.

In arterial blood flow, wall shear stress (WSS) is defined as the tangential force exerted by the blood on the arterial wall per unit area, in the direction of the local tangent plane (Katritsis et al., 2007). WSS is a function of velocity and viscosity of the fluid. In all the cases, flow inside the aneurysm sac results in elevated WSS. It is apparent from the trend in the velocity profile that the increase in the angle of tortuosity increases the maximum velocity in the sac and consequently the maximum wall shear stress (WSS). As the angle of curvature reaches 90˚, the WSS exerted on the sac wall increases and then reduces. This strengthens the fact that the aneurysm sac is more prone to rupture at higher curvatures of the parent vessel. The change in magnitude of WSS is depicted in Fig 11.

Figure 11: Bar Graph depicting the difference in the magnitudes of Maximum WSS and Average WSS with increase in angle of tortuosity of the parent vessel.

4.2 Aneurysmal Hemodynamics due to tortuosity in Parent Artery – Post Stenting

4.2.1 Velocity Reduction

This section determines the effectiveness of the stents in terms of velocity reduction and WSS reduction. The strut height and porosity are varied simultaneously. The strut height ranges from 30 µm to 90 µm, while the width is kept constant at 30 µm. The porosity values range from 60% to 90%, with a 10% increase in each case. Fig 12 shows the contour plot for intra-aneurysmal velocity post-stenting in case of a straight parent vessel. Fig 13 and Fig 14 show the contour plots for intra-aneurysmal velocities in the aneurysmal sac after deploying the stents in parent vessels with the angle of curvature 90˚ and 180˚, respectively.

The rows represent a change in the velocity of blood flow inside the aneurysmal sac, with respect to increase in the strut height. The columns represent the change with respect to increasing porosity. It can be seen from the contour plots that after deployment of the stents the flow stops impinging on the distal wall of the aneurysmal sac. It is regulated to a proximal-to-distal direction of flow with a more distributed flow profile and the velocity of the flow inside the aneurysm reduces comparably. Even when the porosity of the stent increases and the flow starts following the pattern as in the unstented case, the velocity of the flow is significantly reduced. This indicates that with an increase in strut height the velocity reduction is significantly higher, in case of all the FD porosities.

Furthermore, the area at which the flow impinges at the distal wall decreases as the strut height increases. This indicates the reduction in WSS area and thus reduces the risk of rupture of the aneurysm. The trend of velocity reduction is the same in both the tortuous cases as in the straight vessel. But the effect of velocity reduction is slightly lower in the tortuous cases, considering the inertial inlet flow due to the curvature of the artery. The comparison of magnitudes of velocity reduction is further explained in section 4.3.

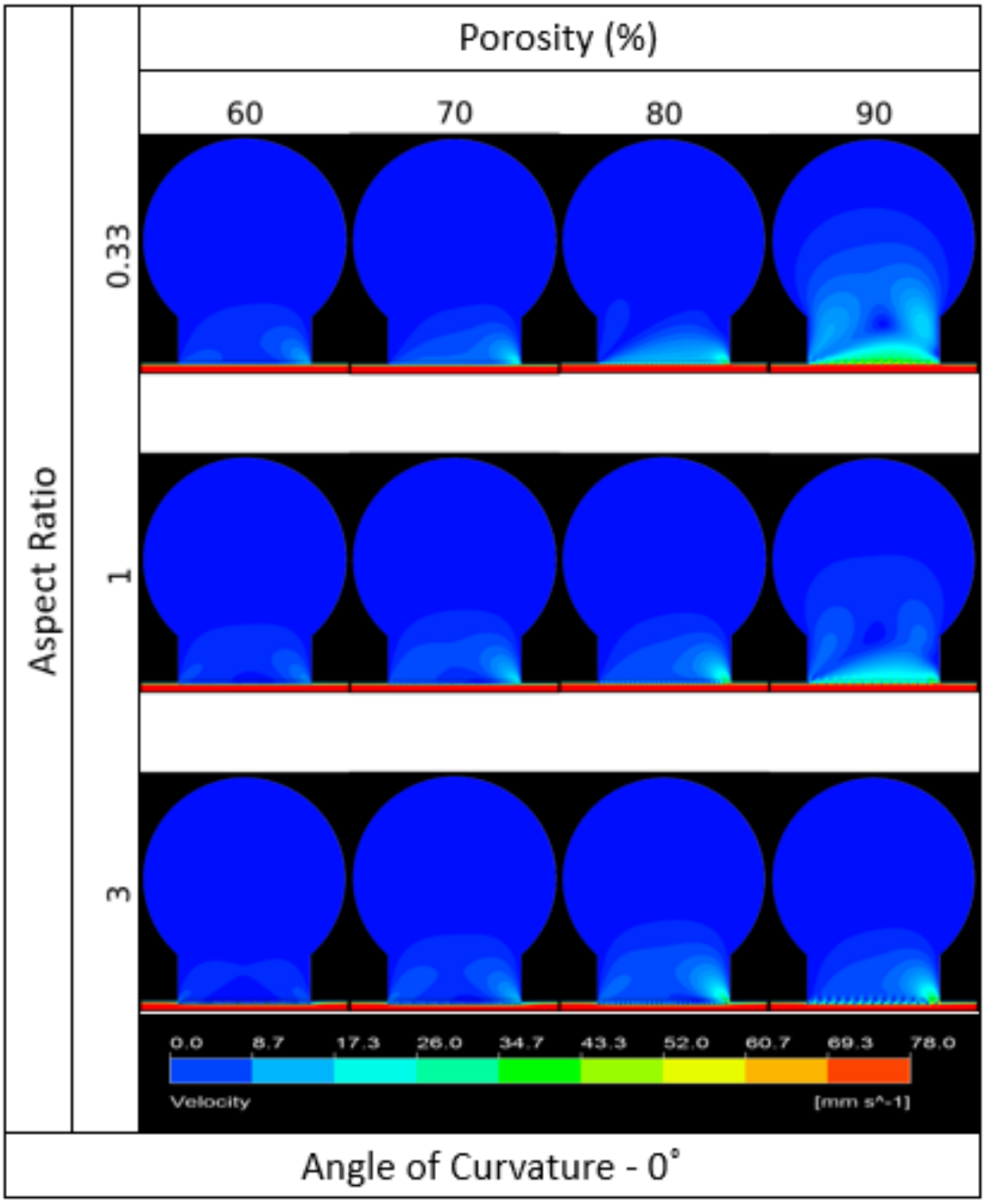

Figure 12: Velocity reduction in the aneurysm sac after deployment of FD in a straight parent vessel. As the strut height increases, the velocity profile shows longitudinal flow distribution across the stent and the flow stops impinging on the distal wall. Same is the case when the porosity of the stent increases.

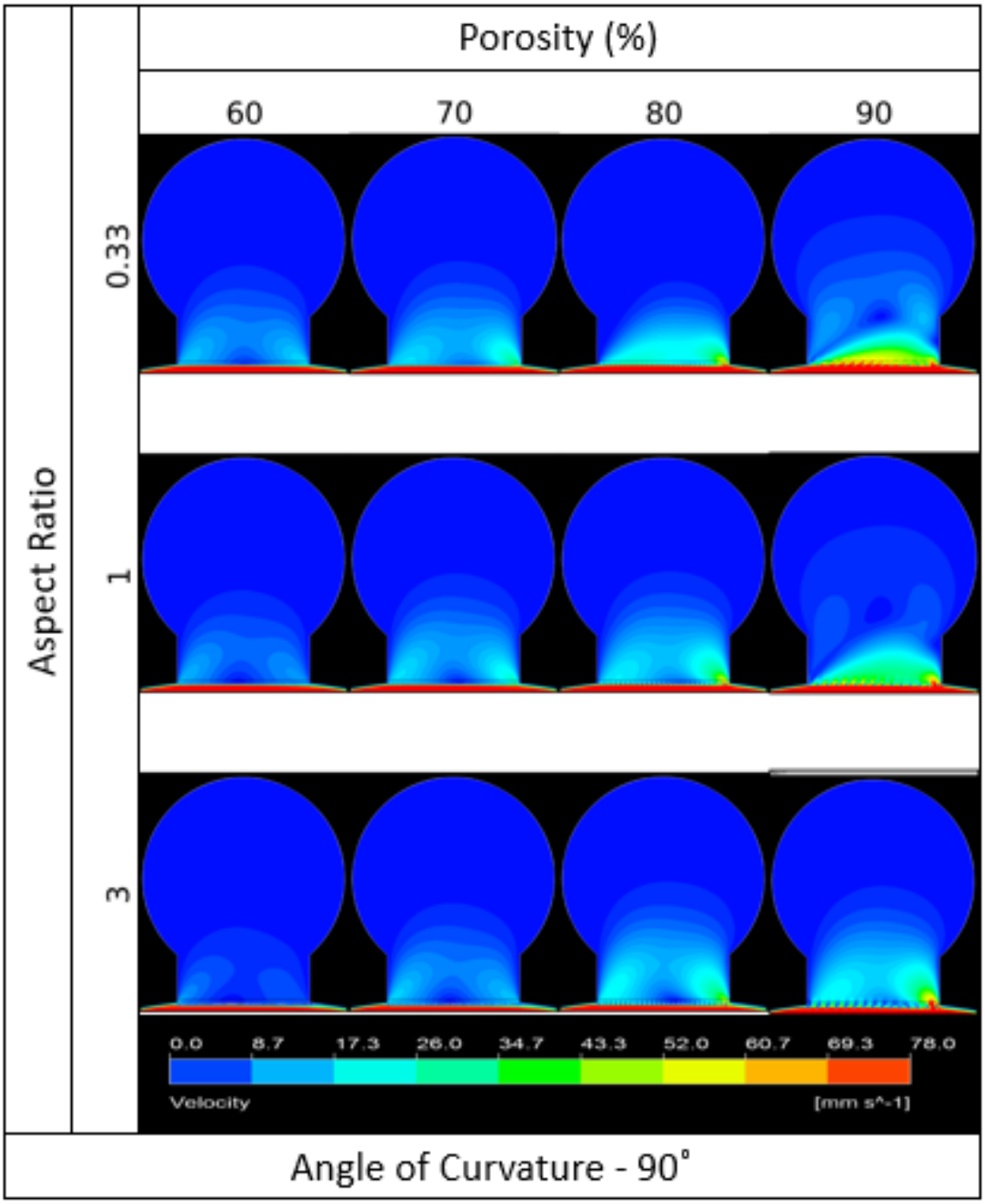

Figure 13: Velocity reduction in the aneurysm sac after deployment of FD in a tortuous parent vessel with angle of curvature of 90˚. As the strut height increases, the velocity profile shows longitudinal flow distribution across the stent and the flow stops impinging on the distal wall. This is also the case when the porosity of the stent increases.

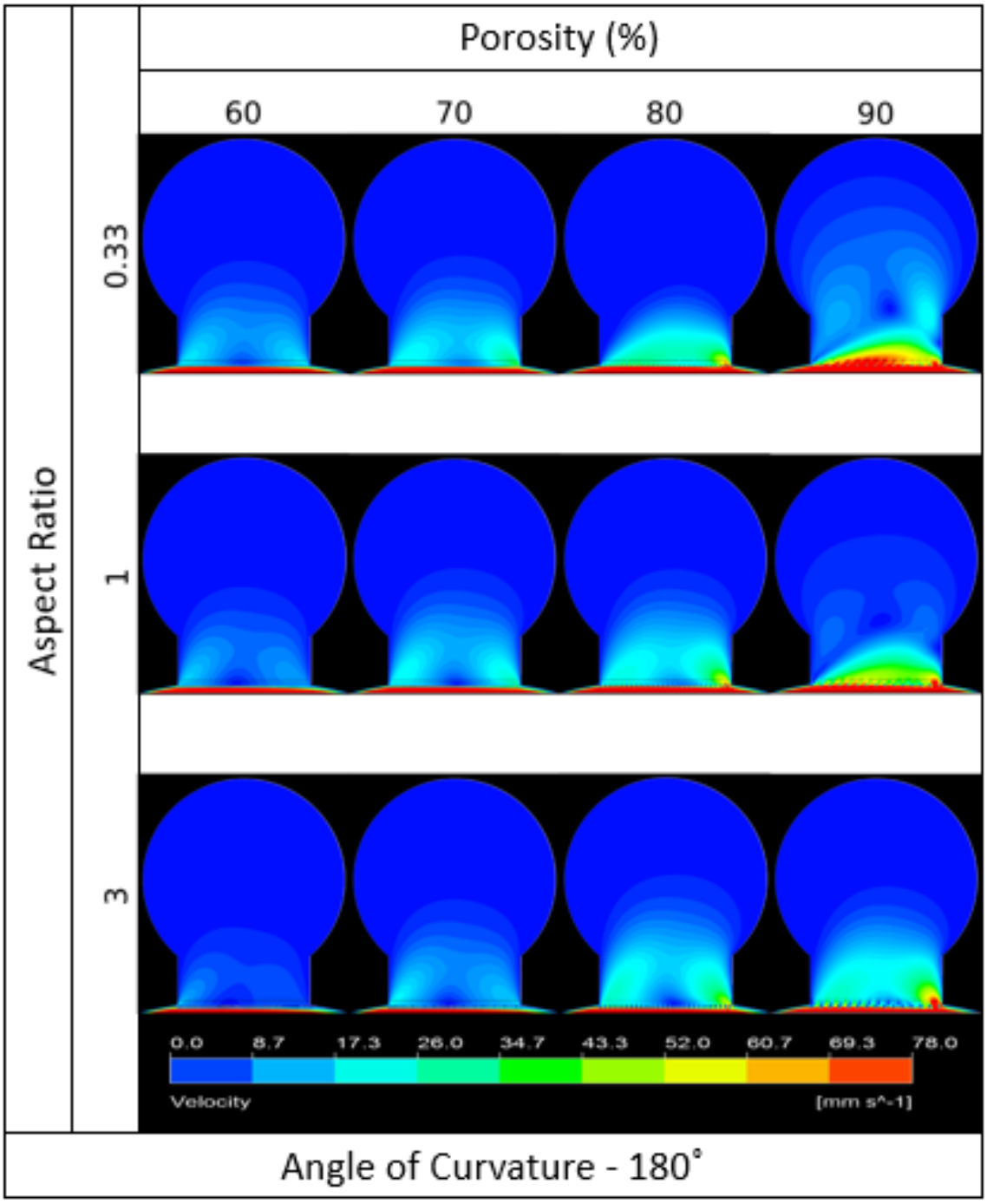

Figure 14: Velocity reduction in the aneurysm sac after deployment of FD in a tortuous parent vessel with angle of curvature of 180˚. As the strut height increases, the velocity profile shows longitudinal flow distribution across the stent and the flow stops impinging on the distal wall. This is also the case when the porosity of the stent increases.

4.2.2 Recirculation

In the case of aneurysmal hemodynamics, the streamlines make it easier to visualize the position of the vortex and in turn the recirculation of blood inside the aneurysm sac. Fig 15 represents streamline plots of the flow inside the aneurysm sac in the case of the straight parent vessel. Fig 16 and 17 are the streamline plots for visualizing the vortex in the aneurysmal sac after deploying the stents, in parent vessels with the angle of curvature 90˚ and 180˚ respectively. The plots follow the same pattern as in section 4.2.1.

As the strut heights increase, the vortex in the sac reduces, which ensures that the recirculation of blood inside the sac reduces. When the porosity of the stents increases, the vorticity inside the aneurysmal sac increases. For taller struts, even with higher porosities, the dimension of the vortex is smaller. This ensures lesser recirculation inside the sac. The decrease in re-circulation aids in thrombosis of the diseased tissue. This indicates that taller struts reduce more flow than smaller ones.

The same trends can be seen in the tortuous cases as in the straight parent vessel. The vortex shifts from the distal side of the aneurysm sac to the proximal side, and the area of vortex reduces as the porosity reduces and the strut height increases. Similar to the velocity reduction, it can be seen that the intra-aneurysmal recirculation in the tortuous cases does not reduce as much as in the straight case. But, it can also be noted that the stents with taller struts do reduce the recirculation in the tortuous cases.

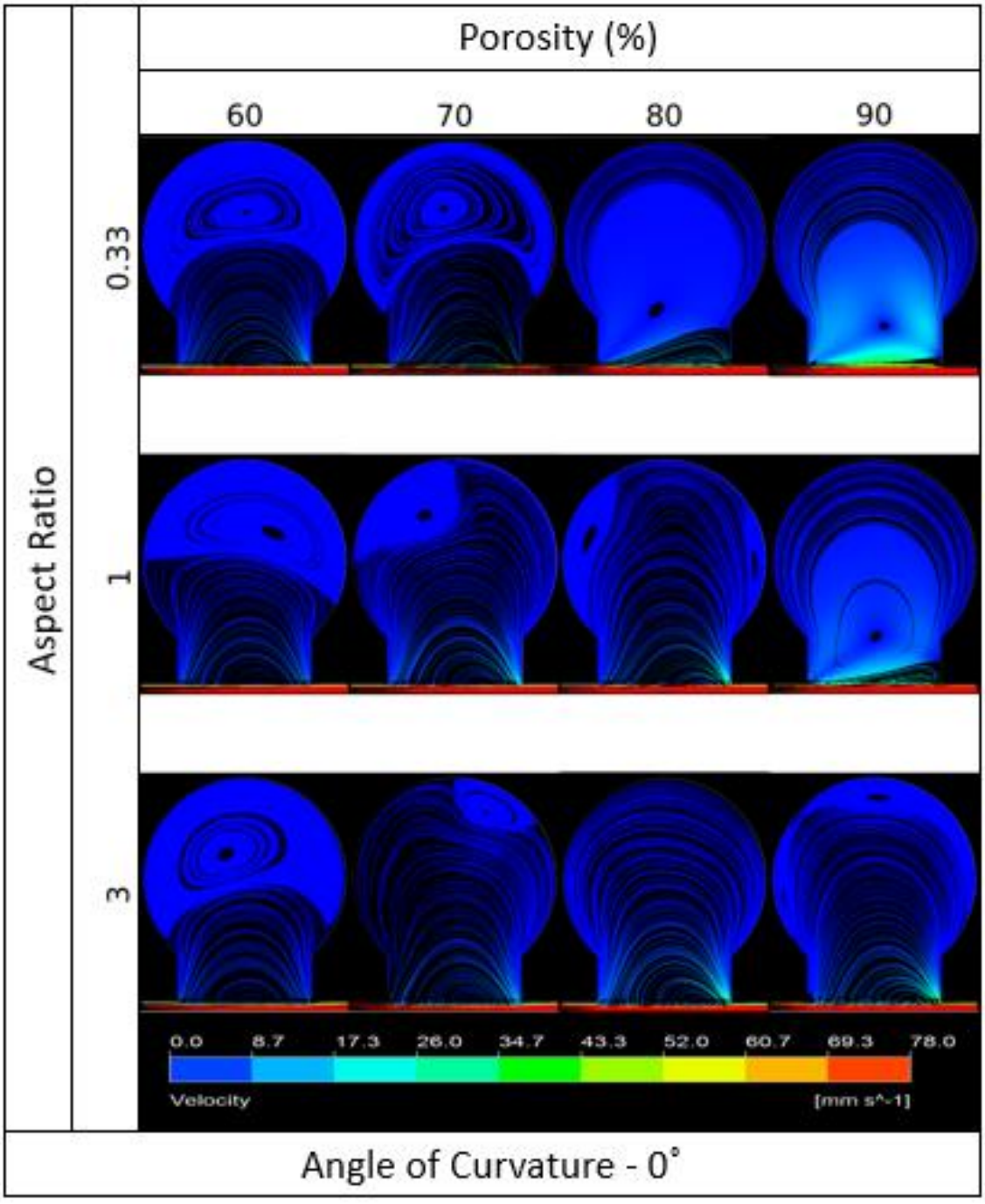

Figure 15: Streamline plot of flow in the aneurysm sac after deployment of FD in a straight parent artery. As the SH increases the vortex inside the aneurysm decreases which indicates reduction of recirculation inside the aneurysmal sac. The results are similar even with increase in the porosity of the stents.

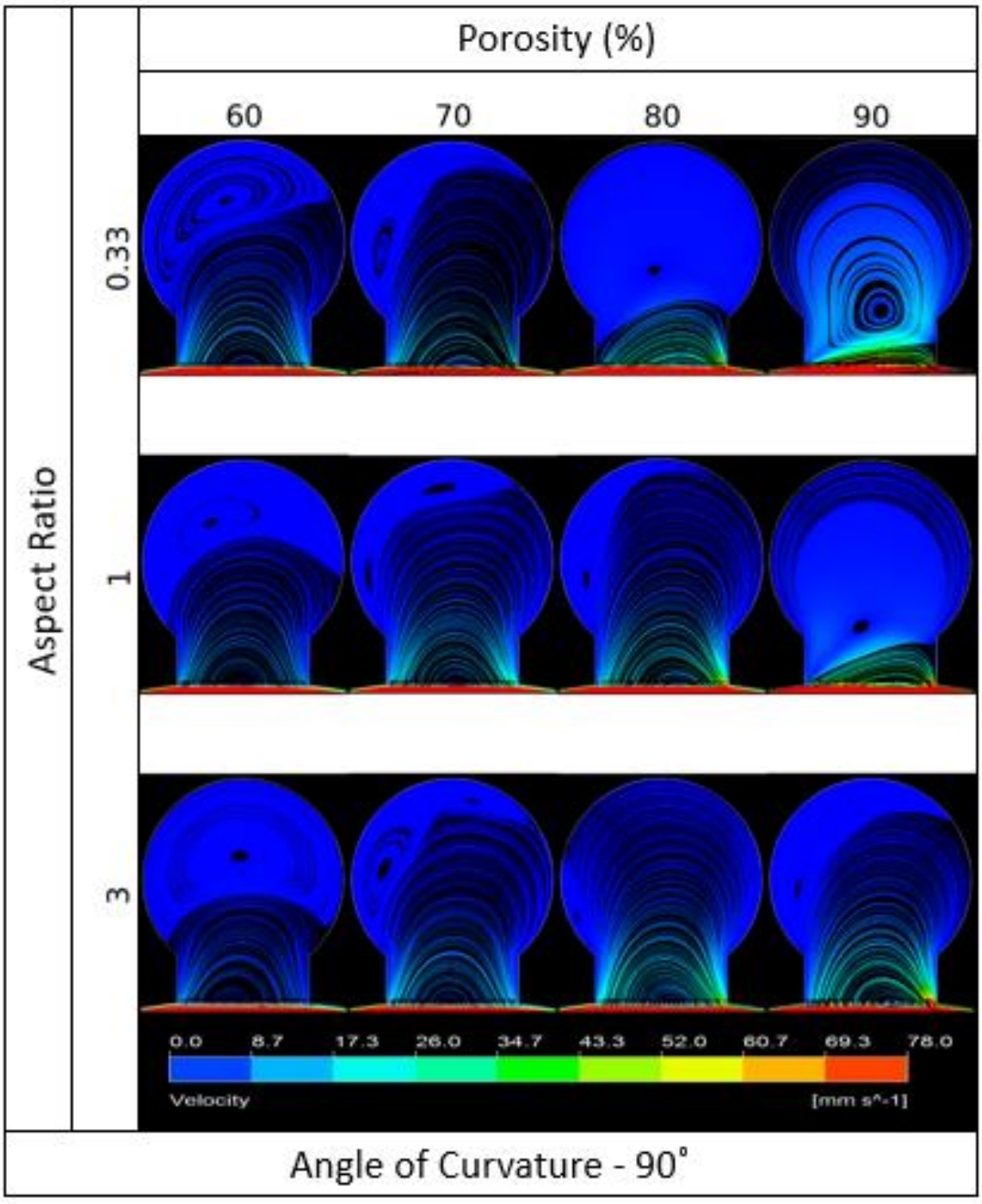

Figure 16*:* Streamline plot of flow in the aneurysm sac after deployment of FD in a tortuous parent vessel with angle of curvature of 90˚. As the SH increases the vortex inside the aneurysm decreases which indicates reduction of recirculation inside the aneurysmal sac. The results are similar even with increase in the porosity of the stents.

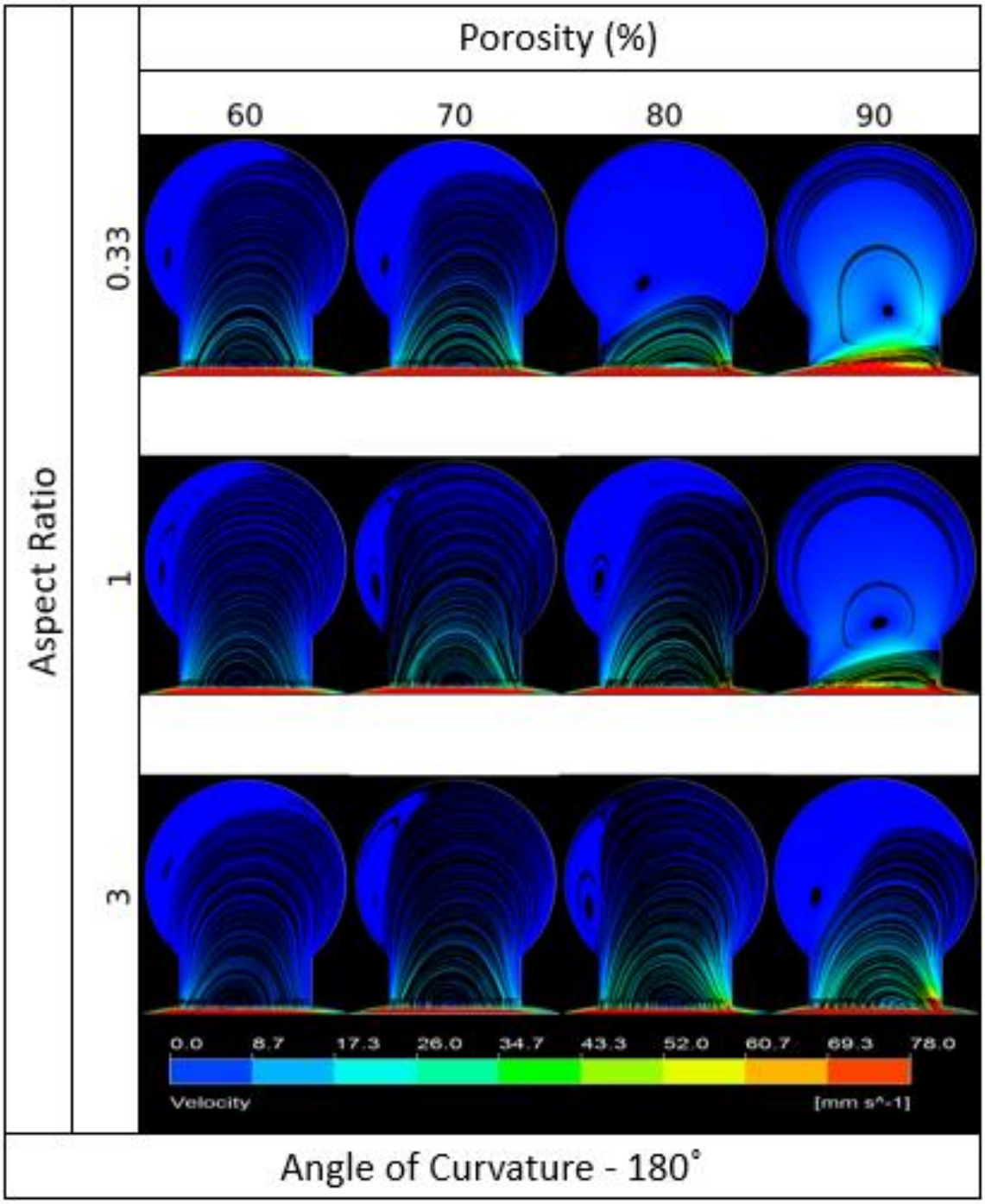

Figure 17: Streamline plot of flow in the aneurysm sac after deployment of FD in a tortuous parent vessel with angle of curvature of 90˚. As the SH increases the vortex inside the aneurysm decreases which indicates reduction of recirculation inside the aneurysmal sac. The results are similar even with increase in the porosity of the stents.

4.3 Effect of Strut Height on Flow Diversion

4.3.1 Velocity Reduction

The effectiveness of the FD can be measured in terms of velocity reduction after deployment of the FD. A decrease in velocity increases the thrombosis inside the aneurysmal sac. Moreover, reduction in velocity lowers the risk of rupture of the aneurysm. Velocity reduction in the aneurysmal sac is expressed as a percentage as given below:

$$\Delta V = \left(\frac{\bar{V}_{US} - \bar{V}_S}{\bar{V}_{US}}\right) \times 100 \,,$$

Where, $\bar{V}_{US}$ and $\bar{V}_S$ are the magnitudes of area weighted average velocities in the aneurysmal sac in unstented and stented cases respectively.

Fig 18 (a), 18 (b), and 18 (c) display the graphs comparing the magnitude of velocity reduction in the sac, at aspect ratio 1/3, 1, and 3 respectively. Each graph compares the velocity reduction with respect to an increase in the porosity and angle of curvature.

As the strut height and in turn the aspect ratio increases the velocity reduction increases. It can be seen, that the velocity reduction is better in case of the struts with aspect ratio 3 than that of the struts with aspect ratio 1/3. The same is true even in the case of higher porosities. Although there is a noticeable difference between the straight and the tortuous case, taller struts are seen to provide more flow reduction in all the cases.

(a)

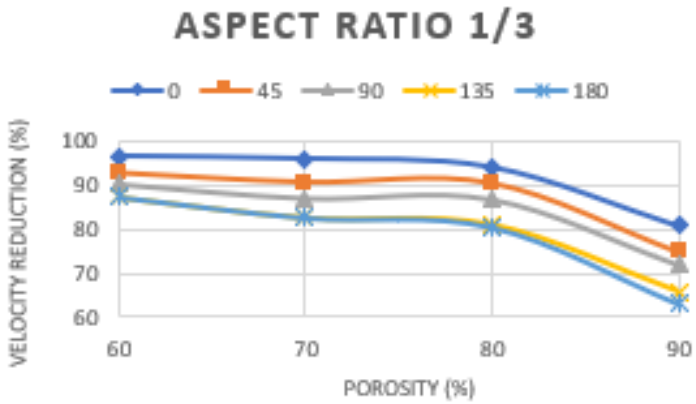

(b)

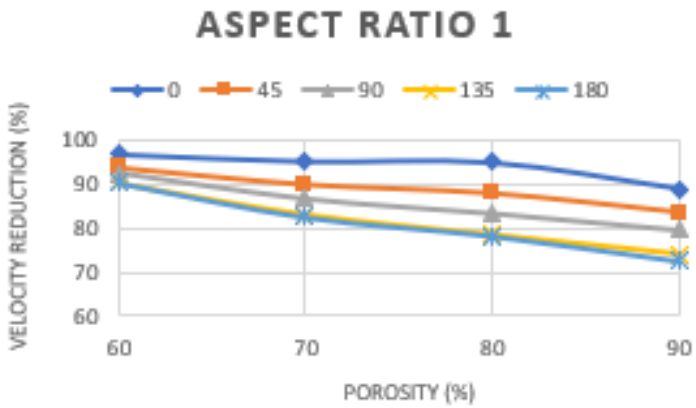

(c)

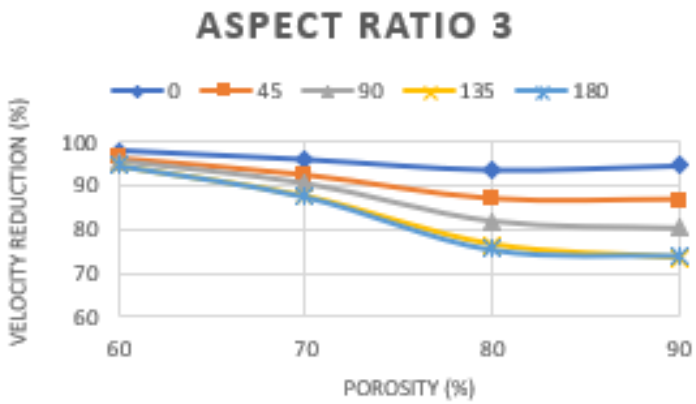

Figure 18: Percentage reduction of velocity in stents with aspect ratio (a) 1/3, (b) 1, and (c) 3. Graphs compare velocity reduction with respect to increasing porosities in each case. As the aspect ratio increases, the velocity reduction is greater even at higher porosities.

4.3.2 WSS Reduction

Another parameter to measure the effectiveness of the FD is WSS reduction. The WSS reduction in the aneurysmal sac is expressed as a percentage as given below:

$$\Delta WSS = \left(\frac{\overline{WSS}_{US} - \overline{WSS}_{S}}{\overline{WSS}_{US}}\right) \times 100 \text{ ,}$$

Where, $\overline{WSS}_{US}$ and $\overline{WSS}_{S}$ are the magnitudes of area weighted average WSS at the aneurysmal sac wall in unstented and stented case respectively.

Fig 19 (a), 19 (b), and 19 (c) display the comparison of WSS reduction in the sac at aspect ratio 1/3, 1 and 3 respectively. Each graph compares the WSS reduction with respect to an increasing porosity and angle of curvature.

The magnitude of WSS is proportional to the velocity gradient near the wall. Thus, low WSS can be obtained at lower velocities. As the WSS at the aneurysmal wall decreases, the area at which the flow impinges on the distal wall of the aneurysm decreases. This reduces the risk of rupture of the aneurysm. As the strut height increases, the percentage reduction in WSS increases. The measure of WSS reduction decreases as the angle of tortuosity increases but it is apparent from the plots that the taller struts perform better even in the most tortuous cases.

(a)

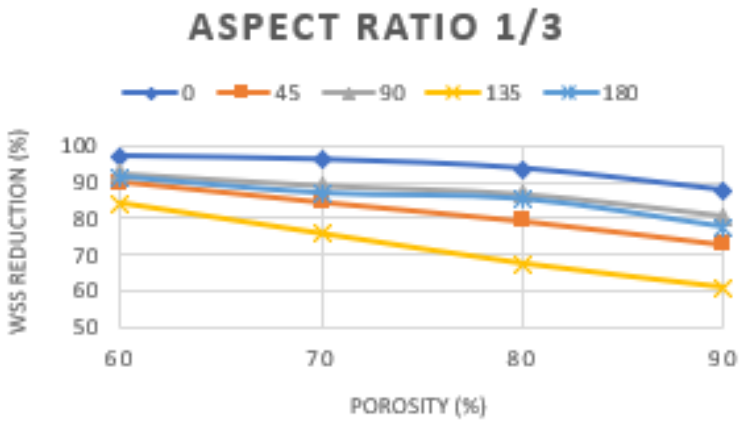

(b)

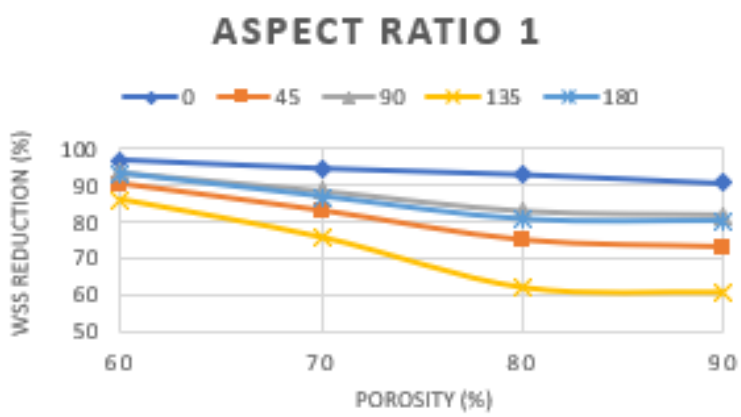

(c)

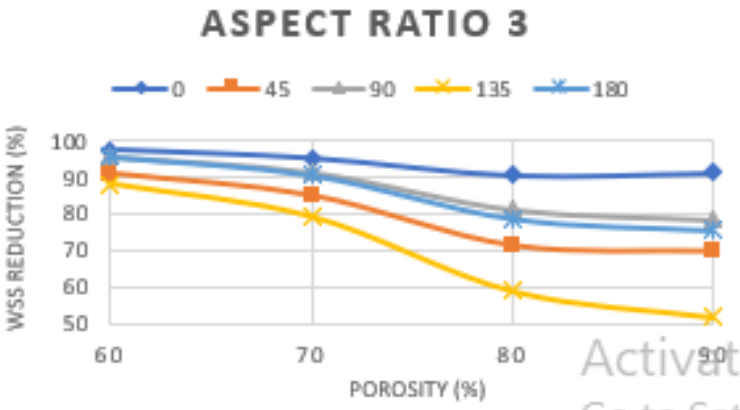

Figure 19: Percentage reduction of WSS in stents with aspect ratio (a) 1/3, (b) 1, and (c) 3. Graphs compare WSS reduction with respect to increasing porosities in each case. As the aspect ratio increases, the WSS reduction is greater even at higher porosities.

5. CONCLUSION

5.1 Concluding Remarks

The main objective of this project was to investigate the effect of taller strut heights on the tortuous cerebral vasculature. For the same, intra-aneurysmal hemodynamics of saccular aneurysms on parent vessel with different tortuosities were computed. After which the intra-aneurysmal hemodynamics were quantified before and after placement of FD's, wherein the strut height and the porosity was altered simultaneously.

Maximum velocity inside the sac increases as the angle of curvature increases within $\alpha \leq 90^{\circ}$ after which it reduces. However, taking in consideration that the flow is inertial as the angle of curvature increases, the velocity of flow inside the aneurysmal sac is greater in the range $90^{\circ} < \alpha \leq 180^{\circ}$ than in the straight case. The weighted average velocity inside the sac decreases gradually as the angle of curvature of the parent vessel increases. Consequently, the results obtained for maximum and weighted average WSS follow the same pattern as the velocity.

After deploying the FDs, the flow stops impinging on the distal wall and passes longitudinally over the device. The maximum, as well as the weighted average velocity inside the aneurysmal sac, decreases considerably. There is a considerable reduction in the maximum and average WSS as well. Although, the flow reduction decreases when the porosity increases, taller struts demonstrate better flow reduction compared to the shorter struts. The velocity and WSS reductions are more effective with an increase in the strut height even in the case of inertial flows and at all the porosities. The findings of this

simulation study suggest that increasing the height of the struts can be a plausible approach to achieve efficient flow reduction in varying parent geometries, specifically in terms of parent tortuosity.

5.2 Limitations of the Study

This study shows the potential of taller struts over the entire range of vessel curvatures based on the study on 2D steady state models. However, for a more accurate understanding of the flow phenomenon, studies on 3D models are recommended. Furthermore, ideal models may help in better understanding the complex flow phenomenon in the worst-case scenarios. CFD simulations are sensitive to even the minute topographic changes in the features of the geometry, thus, using clinically relevant patient-specific models would further reinforce the conclusions of this study.

The study modeled blood as Newtonian and the flow as non-pulsatile. For an accurate comprehension of the aneurysmal hemodynamics, the Non-Newtonian aspect of the blood should be taken into consideration. Moreover, the pulsatility of the blood circulation is also one of the widely used parameters used in a lot of literature. Steady-state is appropriate for estimating maximum values of mechanical parameters, but to predict more complex and transient behavior of the blood circulation (e.g. platelet deposition), pulsatility must be considered. Studies have used a generalized power law to inculcate the pulsatility of the blood flow in the simulations.

Finally, various geometric considerations such as elasticity of vessel walls and varying aneurysm geometry can be advised as the next step in further improving the study. For ease of sorting data, the diameter of the ICA model was taken as the average throughout its length. But, actual ICA geometry is tapered throughout its length. Studying the change in the hemodynamics of the blood vessel and consequently inside the aneurysmal sac as an effect of taper in the geometry would be an interesting problem to look into.

5.3 Future Direction

Conducting CFD studies for 3D models is computationally costly and is difficult on personal computers. Hence, a remote cluster is better suited to run 3D simulations while reducing the computational costs. Good quality of 3D patient-specific aneurysm images can be acquired from digital subtraction angiography and 3D rotational angiographic imaging. Using the patient-specific geometry would restrict the observation to those specific models but would take into consideration the minute details of the morphology of those models. The effect of morphological parameters such as the vessel taper and surface roughness in the vessel can be studied better with this approach. Applying a parabolic flow profile at the inlet instead of using longer parent vessel inlet and outlet lengths can further reduce the computational cost.

The Non-Newtonian nature of blood is significant due to the shear thinning property of viscosity at certain shear rates (Berger & Jou, 2000). Blood can be modeled as Non-Newtonian fluid by using the generalized power law model or the Carreau – Yasuda

model. The generalized power law model takes into consideration the shear thinning as well as the shear thickening behaviors of blood ((Johnston, Johnston, Corney, & Kilpatrick, 2004). While the Carreau – Yasuda model uses viscosity functions which has finite value at both high and low shear (Siebert & Fodor, 2009).

Finally, the effectiveness of the proposed taller struts can be verified for various aneurysm geometries such as fusiform aneurysms and saccular aneurysms at vessel bifurcations. Given that ICA geometry has a lot of perforator arteries, studies should also be considered using a perforator artery in the idealized models. An accumulation of all these parameters would help in better understanding FD as the treatment option for cerebral aneurysms.

6. BIBLIOGRAPHY

Alderazi, Y. J., Shastri, D., Kass-Hout, T., Prestigiacomo, C. J., Gandhi, C. D., Alderazi, Y. J., … Gandhi, C. D. (2014). Flow Diverters for Intracranial Aneurysms, Flow Diverters for Intracranial Aneurysms. *Stroke Research and Treatment, Stroke Research and Treatment*, *2014*, *2014*, e415653. https://doi.org/10.1155/2014/415653, 10.1155/2014/415653

Alkhalili, K., Hannallah, J., Cobb, M., Chalouhi, N., Philips, J. L., Echeverria, A. B., … Fernando, L. (2018). The Effect of Stents in Cerebral Aneurysms: A Review. *Asian Journal of Neurosurgery*, *13*(2), 201–211. https://doi.org/10.4103/1793-5482.175639

An, S. J., Kim, T. J., & Yoon, B.-W. (2017). Epidemiology, Risk Factors, and Clinical Features of Intracerebral Hemorrhage: An Update. *Journal of Stroke*, *19*(1), 3–10. https://doi.org/10.5853/jos.2016.00864

ANSYS Fluent Tutorial Guide. (2015). Retrieved from http://www.ansys.com

Augsburger, L., Farhat, M., Reymond, P., Fonck, E., Kulcsar, Z., Stergiopulos, N., & Rüfenacht, D. A. (2009). Effect of flow diverter porosity on intraaneurysmal blood flow. *Clinical Neuroradiology*, *19*(3), 204–214. https://doi.org/10.1007/s00062-009-9005-0

Benjamin, E. J., Virani, S. S., Callaway, C. W., Chamberlain, A. M., Chang, A. R., Cheng, S., … Muntner, P. (2018). *Heart disease and stroke statistics - 2018 update: A report from the American Heart Association*. *Circulation* (Vol. 137). https://doi.org/10.1161/CIR.0000000000000558

Berger, S. A., & Jou, L.-D. (2000). Flows in Stenotic Vessels. *Annual Review of Fluid Mechanics*, *32*(1), 347–382. https://doi.org/10.1146/annurev.fluid.32.1.347

Castro, M. A., Akan, H., Kim, J. E., & Souftas, V. D. (2013). Understanding the Role of Hemodynamics in the Initiation, Progression, Rupture, and Treatment Outcome of Cerebral Aneurysm from Medical Image-Based Computational Studies Academic Editors, *2013*, 17. https://doi.org/10.5402/2013/602707

Chung, B., & Cebral, J. R. (2014). CFD for Evaluation and Treatment Planning of Aneurysms: Review of Proposed Clinical Uses and Their Challenges. *Annals of Biomedical Engineering*, *43*(1), 122–138. https://doi.org/10.1007/s10439-014-1093-6

Coussement, G., Eker, O. F., Zouaoui Boudjeltia, K., Vanrossomme, A. E., de Sousa, D. R., Bonafé, A., … Courbebaisse, G. (2016). Does the gravity orientation of saccular aneurysms influence hemodynamics? An experimental study with and without flow diverter stent. *Journal of Biomechanics*, *49*(16), 3808–3814. https://doi.org/10.1016/j.jbiomech.2016.10.007

Dandy, W. E. (1938). INTRACRANIAL ANEURYSM OF THE INTERNAL CAROTID ARTERY: CURED BY OPERATION. *Annals of Surgery*, *107*(5), 654–659. Retrieved from http://www.ncbi.nlm.nih.gov/pubmed/17857170

David Fiorella, MD, PhD; Michael E. Kelly, MD; Raymond D. Turner IV, MD; and Pedro Lylyk, M. (2008). Endovascular Treatment of Cerebral Aneurysms (June 2008). Retrieved from https://evtoday.com/2008/06/EVT0608_06.php/

Frösen, J., Tulamo, R., Paetau, A., Laaksamo, E., Korja, M., Laakso, A., … Hernesniemi, J. (2012).

Saccular intracranial aneurysm: pathology and mechanisms. *Acta Neuropathologica*, *123*(6), 773–786. https://doi.org/10.1007/s00401-011-0939-3

Gilroy, A. M., MacPherson, B. R., & Ross, L. M. (2008). *Atlas of anatomy*. Stuttgart ; New York: Thieme. Retrieved from https://ucr.worldcat.org/title/atlas-of-anatomy/oclc/214300025&referer=brief_results

Greving, J. P., Wermer, M. J. H., Brown, R. D., Morita, A., Juvela, S., Yonekura, M., … Algra, A. (2014). Development of the PHASES score for prediction of risk of rupture of intracranial aneurysms: A pooled analysis of six prospective cohort studies. *The Lancet Neurology*, *13*(1), 59–66. https://doi.org/10.1016/S1474-4422(13)70263-1

Guglielmi, G., Viñuela, F., Sepetka, I., & Macellari, V. (1991). Electrothrombosis of saccular aneurysms via endovascular approach. *Journal of Neurosurgery*, *75*(1), 1–7. https://doi.org/10.3171/jns.1991.75.1.0001

ISHIKAWA, T. (2010). What is the Role of Clipping Surgery for Ruptured Cerebral Aneurysms in the Endovascular Era? A Review of Recent Technical Advances and Problems to be Solved. *Neurologia Medico-Chirurgica*, *50*(9), 800–808. https://doi.org/10.2176/nmc.50.800

Jeong, Y. G., Jung, Y. T., Kim, M. S., Eun, C. K., & Jang, S. H. (2009). Size and location of ruptured intracranial aneurysms. *Journal of Korean Neurosurgical Society*, *45*(1), 11–15. https://doi.org/10.3340/jkns.2009.45.1.11

Johnston, B. M., Johnston, P. R., Corney, S., & Kilpatrick, D. (2004). Non-Newtonian blood flow in human right coronary arteries: steady state simulations. *Journal of Biomechanics*, *37*(5), 709–720. https://doi.org/10.1016/J.JBIOMECH.2003.09.016

Katritsis, D., Kaiktsis, L., Chaniotis, A., Pantos, J., Efstathopoulos, E. P., & Marmarelis, V. (2007). Wall Shear Stress: Theoretical Considerations and Methods of Measurement. *Progress in Cardiovascular Diseases*, *49*(5), 307–329. https://doi.org/10.1016/j.pcad.2006.11.001

Keedy, A. (2006). An overview of intracranial aneurysms. *McGill Journal of Medicine*, *9*(2), 141–146.

Kim, M., Taulbee, D. B., Tremmel, M., & Meng, H. (2008). Comparison of Two Stents in Modifying Cerebral Aneurysm Hemodynamics. *Ann Biomedical Engineering*, *36*(5), 726–741. https://doi.org/10.1007/s10439-008-9449-4.Comparison

Kliś, K., Krzyżewski, R., Kwinta, B., Stachura, K., & Gąsowski, J. (2019). Tortuosity of the Internal Carotid Artery and Its Clinical Significance in the Development of Aneurysms. *Journal of Clinical Medicine*, *8*(2), 237. https://doi.org/10.3390/jcm8020237

Korja, M., Kivisaari, R., Rezai Jahromi, B., & Lehto, H. (2016). Size and location of ruptured intracranial aneurysms: consecutive series of 1993 hospital-admitted patients. *Journal of Neurosurgery*, *127*(October), 748–753. https://doi.org/10.3171/2016.9.jns161085

Lauric, A., Hippelheuser, J., Safain, M. G., & Malek, A. M. (2014). Curvature effect on hemodynamic conditions at the inner bend of the carotid siphon and its relation to aneurysm formation. *Journal of Biomechanics*, *47*(12), 3018–3027.

https://doi.org/10.1016/j.jbiomech.2014.06.042

Lin, L. M., Colby, G. P., Jiang, B., Uwandu, C., Huang, J., Tamargo, R. J., & Coon, A. L. (2015). Classification of cavernous internal carotid artery tortuosity: A predictor of procedural complexity in Pipeline embolization. *Journal of NeuroInterventional Surgery*, *7*(9), 628–633. https://doi.org/10.1136/neurintsurg-2014-011298

Lv, N., Cao, W., Larrabide, I., Huang, Q., Liu, J., Fang, Y., … Zhu, D. (2018). Hemodynamic Changes Caused by Multiple Stenting in Vertebral Artery Fusiform Aneurysms: A Patient-Specific Computational Fluid Dynamics Study. *American Journal of Neuroradiology*, *39*(1), 118–122. https://doi.org/10.3174/ajnr.a5452

Mach, G., Sherif, C., Windberger, U., Plasenzotti, R., & Gruber, A. (2016). A Non Newtonian Model for Blood Flow behind a Flow Diverting Stent, 3–6.

Massoud, T. F., Turjman, F., Ji, C., Viñuela, F., Guglielmi, G., Gobin, Y. P., & Duckwiler, G. R. (1995). *Endovascular Treatment of Fusiform Aneurysms with Stents and Coils: Technical Feasibility in a Swine Model*. *AJNR Am J Neuroradiol* (Vol. 16). Retrieved from https://pdfs.semanticscholar.org/367a/0a08f062f9a722b8dd64c98f004fa7c65e0d.pdf?_ga=2.930289.1172673474.1551170513-1388328502.1551170513

Meng, H., Wang, Z., Kim, M., Ecker, R. D., & Hopkins, L. N. (2006). Saccular aneurysms on straight and curved vessels are subject to different hemodynamics: implications of intravascular stenting. *American Journal of Neuroradiology*, *27*(9), 1861–1865. https://doi.org/10.3174/ajnr.a3234

Nelson, P. K., Lylyk, P., Szikora, I., Wetzel, S. G., Wanke, I., & Fiorella, D. (2011). The pipeline embolization device for the intracranial treatment of aneurysms trial. *American Journal of Neuroradiology*, *32*(1), 34–40. https://doi.org/10.3174/ajnr.A2421

Passerini, T., Sangalli, L. M., Vantini, S., Piccinelli, M., Bacigaluppi, S., Antiga, L., … Veneziani, A. (2012). An Integrated Statistical Investigation of Internal Carotid Arteries of Patients Affected by Cerebral Aneurysms. *Cardiovascular Engineering and Technology*, *3*(1), 26–40. https://doi.org/10.1007/s13239-011-0079-x

Peck, R. A. (2015). *Novel Solid Construct Flow Diverter for the Treatment of Intracranial Aneurysms by*. University of California, Riverside.

Pia, H. W. (1980). Large and giant aneurysms. *Neurosurgical Review*, *3*(1), 7–16. https://doi.org/10.1007/BF01644413

Pu, F., Xie, S., Li, D., Li, S., Zhang, C., & Fan, Y. (2012). Geometric classification of the carotid siphon: association between geometry and stenoses. *Surgical and Radiologic Anatomy*, *35*(5), 385–394. https://doi.org/10.1007/s00276-012-1042-8

Riccardello, G. J., Shastri, D. N., Changa, A. R., Thomas, K. G., Roman, M., Prestigiacomo, C. J., & Gandhi, C. D. (2018). Influence of relative residence time on side-wall aneurysm inception. *Clinical Neurosurgery*, *83*(3), 574–581. https://doi.org/10.1093/neuros/nyx433

Savastano, L. E., Bhambri, A., Andrew Wilkinson, D., & Pandey, A. S. (2018). *Biology of Cerebral*

Aneurysm Formation, Growth, and Rupture. *Intracranial Aneurysms*. Elsevier Inc. https://doi.org/10.1016/b978-0-12-811740-8.00002-2

Schievink, W. I. (1997). Intracranial Aneurysms. *New England Journal of Medicine*, *336*(1), 28–40. https://doi.org/10.1056/NEJM199701023360106

Seldinger, S. I. (1953). Catheter Replacement of the Needle in Percutaneous Arteriography: A new technique. *Acta Radiologica [Old Series*, *39*(5), 368–376. https://doi.org/10.3109/00016925309136722

Serbinenko, F. A. (1974). Balloon catheterization and occlusion of major cerebral vessels. *Journal of Neurosurgery*, 125–145. https://doi.org/10.3171/jns.1974.41.2.0125

Siebert, M. W., & Fodor, P. S. (2009). Newtonian and Non-Newtonian Blood Flow over a Backward- Facing Step – A Case Study. *Excerpt from the Proceedings of the COMSOL Conference 2009 Boston*, 5. Retrieved from https://www.comsol.com/paper/download/44844/Fodor.pdf

Skodvin, T. O., Johnsen, L. H., Gjertsen, Ø., Isaksen, J. G., & Sorteberg, A. (2017). Cerebral Aneurysm Morphology before and after Rupture: Nationwide Case Series of 29 Aneurysms. *Stroke*, *48*(4), 880–886. https://doi.org/10.1161/STROKEAHA.116.015288

Torii, R., Oshima, M., Kobayashi, T., Takagi, K., & Tezduyar, T. E. (2007). Influence of wall elasticity in patient-specific hemodynamic simulations. *Computers and Fluids*, *36*(1), 160–168. https://doi.org/10.1016/j.compfluid.2005.07.014

Vega, C., Kwoon, J. V., & Lavine, S. D. (2002). Intracranial aneurysms: Current evidence and clinical practice. *American Family Physician*, *66*(4), 601–608.

Withers, K., Carolan-Rees, G., & Dale, M. (2013). Pipeline TM Embolization Device for the Treatment of Complex Intracranial Aneurysms A NICE Medical Technology Guidance. *Appl Health Econ Health Policy*, *11*, 5–13. https://doi.org/10.1007/s40258-012-0005-x

Xu, X., & Lee, J. S. (2009). Application of the lattice Boltzmann method to flow in aneurysm with ring-shaped stent obstacles. *International Journal for Numerical Methods in Fluids*, *59*(6), 691–710. https://doi.org/10.1002/fld.1829

Zarrinkoob, L., Ambarki, K., Wåhlin, A., Birgander, R., Eklund, A., & Malm, J. (2015). Blood flow distribution in cerebral arteries. *Journal of Cerebral Blood Flow and Metabolism*, *35*(January), 648–654. https://doi.org/10.1038/jcbfm.2014.241

Zhao, X., Li, R., Chen, Y., Sia, S. F., Li, D., Zhang, Y., & Liu, A. (2017). Hemodynamic analysis of intracranial aneurysms using phase-contrast magnetic resonance imaging and computational fluid dynamics. *Acta Mechanica Sinica*, *33*(2), 472–483. https://doi.org/10.1007/s10409-017-0636-0